Electron Impact Excitation of the $1\,^1S \to 3\,^1P$ Transition in Helium

M. A. Khakoo,[1] D. Roundy,[2] and F. Rugamas[1]
[1]Physics Department, California State University, Fullerton, California 92634
[2]Physics Department, University of California, Berkeley, Berkeley, California 94720
(Received 30 January 1995)

In the first direct application of the electron-photon coincidence technique for differential cross-section measurements, experimentally determined ratios of the differential cross sections for the electron impact excitation of the $1\,^1S \to 2\,^1P$ to the $1\,^1S \to 3\,^1P$ transitions are presented at 30 and 40 eV incident electron energies. Differential cross sections for the $1\,^1S \to 3\,^1P$ transitions are derived by normalizing these ratios to available experimental differential cross sections for the $1\,^1S \to 2\,^1P$ transition.

PACS numbers: 34.80.Dp

The electron impact excitation of helium has provided a fertile testing ground for the investigation of fundamental processes. Differential electron scattering using electron energy loss spectroscopy (EELS) has yielded a significant quantity of data concerning both elastic and inelastic electron scattering channels [1]. Excitation of the strong $1\,^1S \to n\,^1P$ transitions in helium has been limited to the energetically resolvable $2\,^1P$ level. There is also a significant body of data of coherence and correlation parameters for the excitation of the $2\,^1P$ and the $3\,^1P$ levels [2,3]. No absolute experimental differential cross sections (DCS's) are available for the excitation of the $n\,^1P$ levels ($n > 2$), the reason being that conventional EELS from gaseous targets (employing electron beams of intensity of several nA) cannot provide the high-energy resolution (<13 meV) required both to resolve the $3\,^1P$ level from nearby levels ($3\,^1D$ and $3\,^3D$) and to provide adequate scattered electron signal for precise DCS measurements.

A semiempirical attempt to obtain DCS's for the $n = 3$ levels, using EELS, used theory [first-order many-body theory (FOMBT)] to calculate the contribution from the $1\,^1S \to 3\,^1D, 3\,^3D$ transitions to the signal [4]. Recently, an 11-state R-matrix calculation [5] was used in astrophysical investigations [6] aiming to determine the H/He ratios of primordial regions of the Universe. Fully experimental DCS's for the $1\,^1S \to 3\,^1P$ transition are thus needed to test present theories.

Here the electron-photon coincidence method is used to enable completely experimental DCS's of the $1\,^1S \to 3\,^1P$ transition to be determined. The present measurements determine the ratios R_p of the DCS's $[d\sigma/d\Omega_e\,(E_0,\theta_e)]$ for the electron impact excitation of $1\,^1S \to n\,^1P$ ($n = 2,3$), i.e.,

$$R_p = \frac{d\sigma/d\Omega_e\,(E_0,\theta_e)\,|2\,^1P}{d\sigma/d\Omega_e\,(E_0,\theta_e)\,|3\,^1P}\,, \qquad (1)$$

at a given incident electron energy (E_0) and scattering angle (θ_e). Using these ratios the DCS's for the $1\,^1S \to 3\,^1P$ transition may be determined by normalization of R_p to the DCS's for $1\,^1S \to 2\,^1P$. Our experimental determination of R_p using the electron-photon coincidence technique relies on the fact that the helium atomic levels are fully LS coupled. Thus for excitation of the singlet $\to$ singlet transitions by electrons, spin interactions are negligible. Also, the excited $n\,^1P$ state in the natural frame coordinates (Fig. 1) can be written as [2]

$$|n\,^1P\rangle = f_{-1}^n|1,-1\rangle + f_1^n|1,1\rangle\,, \qquad (2)$$

where f_{-1}^n and f_1^n are the (complex) scattering amplitudes describing the excited state in the $|L, m_L\rangle$ orbital basis ($L = 1$, $m_L = 1, 0, -1$) with the axis of quantization perpendicular to the scattering plane. The resulting excited state charge distribution $\langle n\,^1P\,|\,n\,^1P\rangle$ has the same reflection symmetry (+ with respect to the scattering plane) as the ground state (isotropic) charge distribution $\langle n\,^1S\,|\,1\,^1S\rangle$. The scattering amplitudes depend on the electron collision dynamics, i.e., the initial and final scattered electron momenta, or, alternatively, E_0 and θ_e.

The electron-photon coincident rate dN_c/dt for any transition can be written as [7]

$$dN_c/dt = d\sigma/d\Omega_e\,(E_0,\theta_e)\{I_e N_G L_e \Delta\Omega_e \Delta\Omega_\gamma\} \times E_e E_\gamma \zeta(\theta_\gamma, \Phi_\gamma)\,. \qquad (3)$$

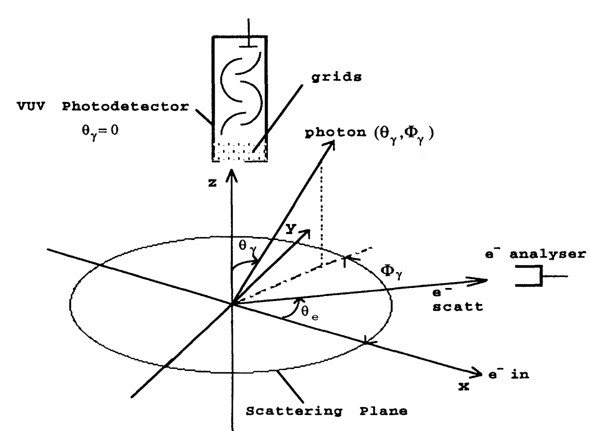

FIG. 1. The scattering geometry for the present eletcron-photon coincidence experiment, shown in the "natural" frame.

I_e, N_G, L_e, $\Delta\Omega_e$, and $\Delta\Omega_\gamma$ are, respectively, the incident electron current (s^{-1}), target gas number density (cm^{-3}), "effective" path length of electrons through the gas target beam (cm), and electron analyzer and photon detector solid angles (sr). E_e and E_γ are the respective detection efficiencies for electrons and photons, and β_γ is the branching ratio for the observed radiation. Again, $d\sigma/d\Omega_e$ is the excitation DCS ($cm^2\,sr^{-1}$). $\zeta(\theta_\gamma, \Phi_\gamma)$ is the angular distribution function of coincident photons from the coherent, excited state. For the $1\,^1S \rightarrow n\,^1P$ transitions in helium at a fixed θ_e^2

$$\zeta(\theta_\gamma, \Phi_\gamma) = \tfrac{1}{2}(3/8\pi)[1 + \cos^2\theta_\gamma - P_1\cos 2(\Phi_\gamma - \gamma)\sin^2\theta_\gamma] \quad (4)$$

with $P_L = 2|f_1^n||f_{-1}^n|$ and $\langle f_1^n f_{-1}^{n*}\rangle = -\frac{1}{2}P_L\exp(-2i\gamma)$. γ is the alignment angle of the exited state charge distribution [2]. When $\theta_\gamma = 0$, i.e., the photons are observed perpendicular to the scattering plane (see Fig. 1), $\zeta(0, \Phi_\gamma) = 3/8\pi$ and the coincidence rate given by Eq. (3) is directly proportional to the excitation DCS $d\sigma/d\Omega_e(E_0, \theta_e)$ if the photon detector is polarization insensitive (otherwise coincident measurements should be taken at two orthogonal values of Φ_γ and summed).

Our method is to take such electron-photon coincidence spectra for the $\theta_\gamma = 0$ setup, for the $1\,^1S \rightarrow 2\,^1P$ and $1\,^1S \rightarrow 3\,^1P$ transitions in helium under identical conditions [identical parameters in {} in Eq. (3)] and known times Δt_1 and Δt_2. Corrected for detector efficiencies, the counts N_c under these coincidence peaks yield

$$\frac{N_c(2\,^1P)/\Delta t_1}{N_c(3\,^1P)/\Delta t_2} = \frac{d\sigma/d\Omega_e(E_0, \theta_e)\,|2\,^1P}{d\sigma/d\Omega_e(E_0, \theta_e)\,|3\,^1P} = R_p \quad (5)$$

from Eq. (3). These R_p ratios can be used to determine $d\sigma/d\Omega_e(E_0, \theta_e)\,|3\,^1P$ using $d\sigma/d\Omega_e(E_0, \theta_e)\,|2\,^1P$ from a conventional EELS experiment.

In our setup, a monochromated electron beam crosses a gas jet from a molybdenum needle. The vacuum was maintained by an unbaffled Diffstak pump with Santovac oil, backed by a rotary pump using a low-grade diffusion pump oil (Diffoil 20, K. J. Lesker Co., vapor pressure $\approx 10^{-7}$ torr) and equipped with a micromaze oil vapor trap. The electron spectrometer has been discussed previously [8]. Scattered electrons are detected as a function of energy loss ΔE and θ_e by a hemispherical analyzer equipped with a high-count-rate electron multiplier [Equipe Thermodynamique et Plasmas (ETP) model AF151]. The electron spectrometer has virtual apertures of 1.5 mm diameter and an energy resolution varying from 120 to 200 meV, an angular resolution of 5° (FWHM), with a current in the range of 0.1 to 0.5 uA. Perpendicular to the scattering plane is the vacuum ultraviolet (vuv) photodector (an electron multiplier with aluminum dynodes ETP AF150), which has three 91% transparency molybdenum grids. The first and third are shorted to the collision region and the second is at +1.5 V (relative to the collision region) to repel helium ions. The dynode of the multiplier is at $-E_0 - 5$ V (relative to the collision region) to repel electrons from reaching it. An in-vacuum stepper motor was used to rotate the photodetctor about the angle Φ_γ (Fig. 1) to determine its polarization efficiency. The gas jet is angled at 45° relative to the scattering plane to shoot the thermal beam of helium downwards, reducing the possibility of detecting neutral $2\,^1S$ or $2\,^3S$ metastables by the photodetector. The timing response and count-rate performance of the photodetectors were <10 ns (pulse width, FWHM), a jitter time of ≈ 1 ns, and an observed count-rate linearity in excess of 100 kHz. The experiment was baked at 120 °C (including the detectors) and performed stably for periods of greater than six months. Typical count rates varied from ≈ 10 to ≈ 2 kHz in the photon channel and ≈ 50 kHz to 100 Hz in the electron channel. The gas source drive pressure was kept below 0.8 torr and this closely corresponded linearly to a pressure of 8×10^{-7} torr in the experimental chamber (corrected for the sensitivity of the ionization gauge). After tuning the electron spectrometer to achieve as well as possible the desired flat ionization energy loss profile [9] at 30 eV impact energy (to get a uniform analyzer transmission), we acquired repetitive coincidence spectra at the energy loss values of 21.212 ± 0.001 eV ($2\,^1P$) and 23.0805 ± 0.001 eV energy loss ($3\,^1P$). The respective times spent at these energy loss values were $\Delta t_1 = 2$ min and $\Delta t_2 = 8$ min per period to acquire about equal statistics for the $2\,^1P$ and $3\,^1P$ coincidence spectra.

A sample of these coincidence spectra is shown in Fig. 2. The "$3\,^1P$" spectrum contains contributions due to the $3\,^1D$ and $3\,^1S$ states which cascade down to the ground state via the $2\,^1P$ state, releasing 58.4 nm photons, detected by our photon detector. The spectrum in Fig. 2(b) was thus deconvoluted for these cascades [10]. The time dependence of this spectrum,

$$G(t) = A_1\int_{-\infty}^{t} e^{-t'/\tau 1}\mathbf{F}(t')\,dt' + A_2\int_{-\infty}^{t} e^{-t'/\tau 4}\,dt' \times \int_{-\infty}^{t'} e^{-t''/\tau 2}\mathbf{F}(t'')\,dt'' + A_3\int_{-\infty}^{t} e^{-t'/\tau 4}\,dt' \times \int_{-\infty}^{t'} e^{-t''/\tau 3}\mathbf{F}(t'')\,dt'', \quad (6)$$

where $\mathbf{F}(t)$ is the instrumental time response, derived from the corresponding $2\,^1P$ coincidence spectrum. The A_i amplitudes are determined from a nonlinear least squares fitting of the "$3\,^1P$" coincidence spectrum. Values for $\tau 1$, $\tau 2$, $\tau 3$, and $\tau 4$ (respectively, the lifetimes of the $3\,^1P \rightarrow 1\,^1S$, $3\,^1D \rightarrow 2\,^1P$, $3\,^1S \rightarrow 2\,^1P$, and $3\,^1P \rightarrow 1\,^1S$ decays) used were 1.77, 15.67, 55.2, and 0.55 ns as given by Wiese, Smith, and Glennon [11]. A typical fit is shown in Fig. 2(b). The resulting areas of the $2\,^1P$ and "$3\,^1P$" peaks are corrected for branching ratios β_γ according to Eq. (3) and the relative photon detector wavelength efficiency at 53.7 and 58.4 nm. The relative photon detector efficiency ratios were measured by carrying out the same coincidence experiment at $E_0 = 100$ eV and small $5° < \theta_e < 20°$ and

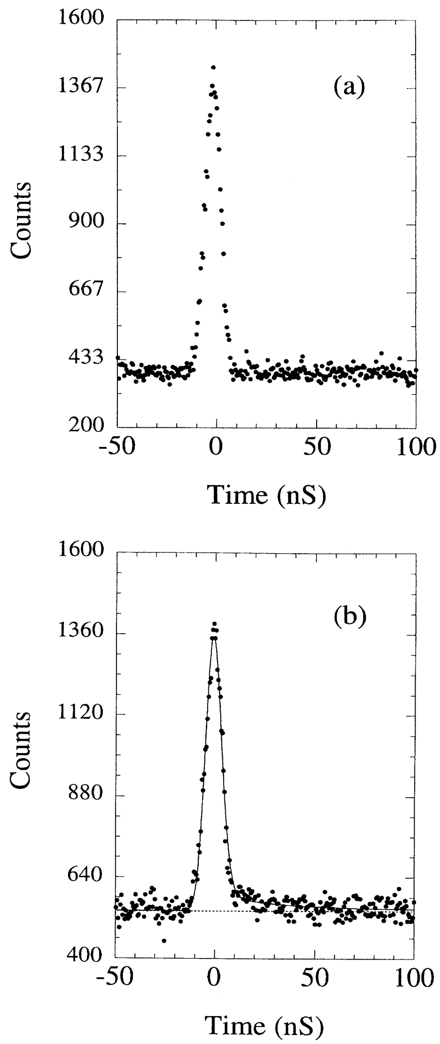

FIG. 2. Electron-photon coincidence spectrum at 40 eV and 20°. (a) The $1\,^1S \rightarrow 2\,^1P$ transition at 40 eV and 20° and (b) the $1\,^1S \rightarrow 3\,^1P$ transition with the fit (solid line) using Eq. (6).

using available theoretical values [12–15] of the ratios of $1\,^1S \rightarrow 2\,^1P$ and $1\,^1S \rightarrow 3\,^1P$ DCS's (which are all in very good agreement in this range). The resulting ratio of relative efficiencies for the 58.4 and 53.7 nm vuv radiation was found to be 1.12 ± 0.02 an in very good agreement with measurements taken at the National Institute of Standards and Technology for the type of surface (Al_2O_3) used for the first dynode of the detector [16], i.e., 1.13 ± 0.02. The polarization efficiency of our detector was determined by taking $2\,^1P$ coincidence spectra at orthogonal values of Φ_γ, i.e., separated by 90°, and correcting these for the total photon signal. This polarization efficiency was consistently found to be <1%. Finally, the ratios of the areas of the $2\,^1P$ coincidence spectrum and the deconvoluted $3\,^1P$ spectrum need to be corrected for radiation trapping effects. We restricted these measurements to $\theta_e < 30°$ since we found that R_p decreases with pressure, independent of θ_e, in the low pressure domain employed here. Typical corrections for the reduction of R_p were in the region of 3–6% in the range of chamber pressures used here, i.e., 3×10^{-6} to 8×10^{-7} torr. We did not correct for the variation of lifetime with pressure [17] as this is negligible in the present domain.

Our final corrected ratios R_p and errors are given in Fig. 3. In Fig. 3(a), we see that the R-matrix theory [5] is not reliable at these energies. The FOMBT [12] provides a good shape but overestimates the value of R_p by ~10%. The distorted wave Born approximation (DWBA) [13] gives good values at small θ_e but above 50° deviates from our values of R_p. The recent convergent close coupling calculations (CCC) of Bray, Fursa, and McCarthy [14] provide the closest agreement with our results and, in fact, are in excellent agreement at $\theta_e > 50°$. The situation at 40 eV [Fig. 3(b)] is similar in that agreement between experiment and theory is best for the CCC. The CCC is the only theory to display the hump in R_p at around 50° as observed (more strongly) in our experiment. The present

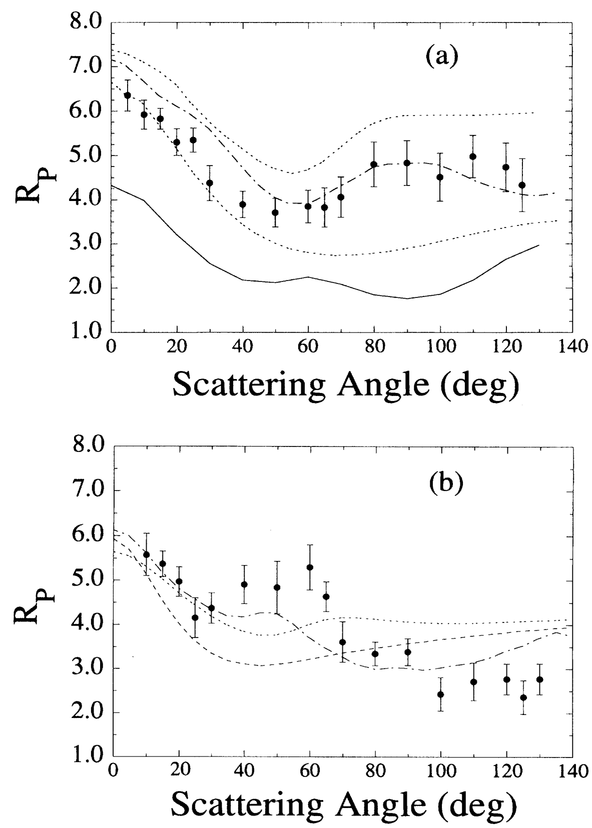

FIG. 3. Ratios R_p at (a) 30 eV and (b) 40 eV impact energy. Legend is ● present experimental values. Theory: --- DWBA; ··· FOMBT; — R-matrix; -·-· CCC.

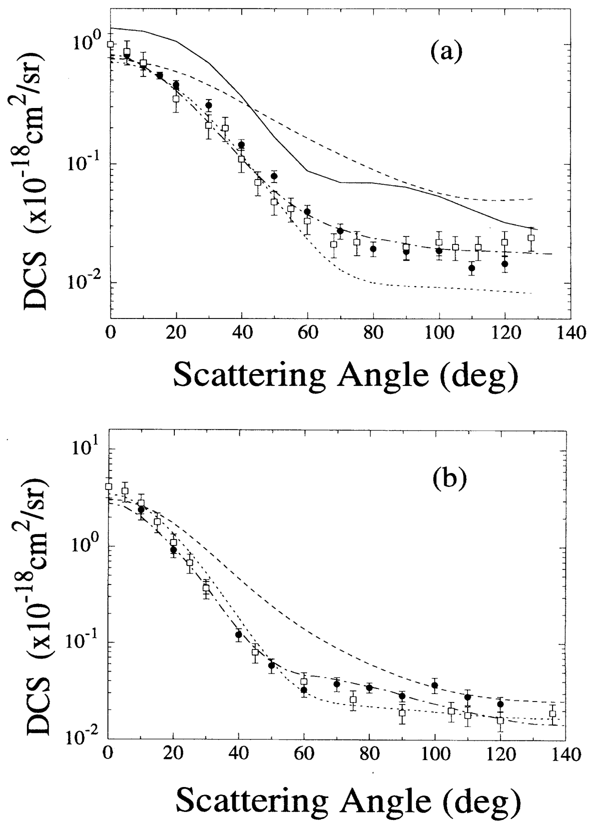

FIG. 4. Normalized DCS's for the $1\,^1S \rightarrow 3\,^1P$ transition at (a) 30 eV and (b) 40 eV impact energy. See text for additional discussion. Legend same as Fig. 3 except squares are $1\,^1S \rightarrow 3\,^1P + 3\,^1D + 3\,^3D$ DCS's of Ref. [4].

CCC results have not yet been tested for convergence, with increasing number of states, regarding these very sensitive R_p values. The FOMBT and DWBA theories give good agreement with experiment for $\theta_e < 40°$.

The DCS's for the $1\,^1S \rightarrow 3\,^1P$ transition (see Fig. 4) are obtained from our R_p ratio values using a weighted average of available experimental $1\,^1S \rightarrow 2\,^1P$ DCS's from the work of Refs. [12], [15], and [18]. Comparisons of the DCS's result in similar conclusions as the R_p values. Also shown are the $1\,^1S \rightarrow 3\,^1P + 3\,^1D + 3\,^3D$ DCS's measured by Chutjian and Thomas [4], which show the dominance of the $3\,^1P$ excitation channel.

This work was supported by the National Science Foundation, under Grant No. NSF-RUI-PHY-9205423. Discussions with and suggestions from Dr. S. Trajmar, Dr. G. Csanak, Dr. T. J. Gay, Dr. E. J. Mansky, Dr. P. Hammond, Dr. D. Madison, Dr. A. Crowe, Dr. J. F. Williams, and Dr. I. Bray are gratefully acknowledged.

[1] S. Trajmar and I. Kanik, in "Atomic Molecular Processes in Fusion Edge-Plasmas," edited by R. K. Janev (Plenum Press, New York, to be published).

[2] N. Andersen, J. W. Gallagher, and I. V. Hertel, Phys. Rep. **165**, 1 (1988).

[3] K. Becker, A. Crowe, and J. W. McConkey, J. Phys. B **25**, 3885 (1992).

[4] A. Chutjian and L. D. Thomas, Phys. Rev. A **11**, 1583 (1975).

[5] W. C. Fon, K. A. Berrington, and A. E. Kingston, J. Phys. B **21**, 2961 (1988).

[6] G. J. Ferland, Astrophys. J. **310**, L67 (1987); B. E. J. Pagel and E. A. Simonson, Rev. Mex. Astron. Astrofis. **18**, 153 (1989).

[7] J. Slevin, Rep. Prog. Phys. **47**, 461 (1984).

[8] M. A. Khakoo, T. Jayaweera, S. Wang, and S. Trajmar, J. Phys. B **26**, 4845 (1993).

[9] J. Nickel, P. W. Zetner, G. Shen, and S. Trajmar, J. Phys. E **22**, 730 (1989).

[10] H. B. van Linden van den Heuvell, E. M. van Gasteren, J. van Eck, and H. G. M. Heideman, J. Phys. B **16**, 1619 (1983).

[11] W. Wiese, M. W. Smith, and B. M. Glennon, *Atomic Transition Probabilities* (NSRDS-NBS, Washington D.C., 1966), Vol. 1.

[12] D. C. Cartwright, G. Csanak, S. Trajmar, and D. F. Register, Phys. Rev. A **45**, 1602 (1992); D. C. Cartwright (private communication).

[13] K. Bartschat and D. H. Madison, J. Phys. B **20**, 153–170 (1988); D. H. Madison (private communication).

[14] I. Bray, D. V. Fursa, and I. E. McCarthy, Phys. Rev. A **51**, 500 (1995); I. Bray, D. V. Fursa, and I. E. McCarthy, J. Phys. B **27**, L421 (1994).

[15] M. J. Brunger, I. E. McCarthy, K. Ratnavelu, P. J. O. Teubner, A. M. Weigold, Y. Zhou, and L. J. Allen, J. Phys. B **23**, 1325 (1991); I. McCarthy (private communication).

[16] L. Randall Canfield and Nils Swanson, J. Res. Natl. Bur. Stand. **92**, 97 (1987).

[17] J. F. Williams, R. Hippler, J. B. Wang, A. G. Micosza, and A. B. Wedding, Phys. Rev. Lett. **69**, 757 (1992); A. G. Micosza, R. Hippler, J. B. Wang, J. F. Williams, and A. B. Wedding, J. Phys. B **27**, 1429 (1994).

[18] D. G. Trulhar, S. Trajmar, W. Williams, S. Ormonde, and B. Torres, Phys. Rev. A **8**, 1602 (1973).